A Concurrent Design Methodology for Grid-Current Feedback Active Damping for LCL-Based Grid-Tied Voltage-Source Converter

Jiazhi Liang, Student Member, IEEE, Jiuchun Jiang, Senior Member, IEEE
National Active Distribution Network Technology Research Center
Collaborative Innovation Center of Electric Vehicles in Beijing
Beijing Jiaotong University
Beijing, P.R. China
jiazliang@bjtu.edu.cn, jcjiang@bjtu.edu.cn

Olorunfemi Ojo, Fellow, IEEE, Josiah Haruna, Student Member, IEEE
Department of Electrical and Computer Engineering
Tennessee Technological University
Cookeville, TN 38505, USA
JOjo@tntech.edu, joharuna42@students.tntech.edu

***Abstract*—A novel concurrent scheme of current control with active damping for LCL-based grid-tied voltage source converter has been proposed based on the D-decomposition methodology. By using the grid-current feedback only, the paper demonstrates that grid-current feedback technique provides a satisfactory system performance, regardless of the resonance frequency of the filter. It also can readily satisfy the relative stability required such as phase margin (PM) and gain margin (GM) by considering gain parameters simultaneously for the two-loop control scheme. The proposed design method is quite simple to implement, without the need of expert knowledge-based parameter tuning. Simulation and experimental results have demonstrated the validity and effectiveness of the proposal.**

Keywords—active damping; grid-current feedback; LCL-filter; voltage source converter

I. INTRODUCTION

LCL resonance has been one of the most important concerns for LCL-based voltage-source-converter [1]. Although many literatures [2-6] have proven that an LCL-filter with a high-frequency / low-frequency resonance can be stabilized with the grid-current / converter-current feedback only, drifting system parameters affect the resonance frequency significantly. For the sake of controllability and robustness, a damper control is usually incorporated. A physical passive damper, such as a resistor in series with the filter capacitor [1], however causes a power loss and reduces the high-frequency attenuation of LCL-filter. Active dampers [7-15] therefore are considered as the promising way at the present time. One conventional way to actively damp the resonance is to feedback an extra current [7-9] or voltage [10] of the filter capacitor. Another way is to develop a robust active damping technique that relies only on the grid-current feedback [11-15], in which no additional sensor is needed. For the second active damping technique, a first-order High-Pass-Filter (HPF) is introduced as an active damper in [12-14]. To obtain a good system dynamic response, the active damper and the current controller must be concurrently designed. So far, these two control loop designs are done sequentially. In [12-15], the current controller is designed first based on the so-called optimum design method proposed in paper [7], which can only provide an approximate calculation for controller gains without taking into consideration the active damper. Hence in reference [15], it is concluded that a poor dynamic response of closed-loop system will be obtained when an active damper of High-Pass-Filter is used to control a low resonance-frequency LCL-filter. This paper provides a new method to design an active damper and a current controller simultaneously in a graphical way for grid-current feedback active damping LCL-based converter. Simulation and experimental results demonstrate that the grid-current active damping technique gives satisfactory performance independent of the ratio between the resonance frequency and the sampling frequency of the LCL-filter.

II. SYSTEM DESCRIPTION

A. Coordinate Transformations

For a balanced system, the three-phase quantities can be modeled as equivalent two-phase quantities in $\alpha\beta$-frame, by disregarding zero-sequence components. Based on the transformation matrix, complex vector associated with a set of phase quantities $\{u_a, u_b, u_c\}$ can be given by

$$u_{\alpha\beta} = u_\alpha + ju_\beta = \frac{2}{3}\left(u_a + e^{j\frac{2\pi}{3}}u_b + e^{-j\frac{2\pi}{3}}u_c\right) \tag{1}$$

$$\begin{bmatrix} u_\alpha \\ u_\beta \end{bmatrix} = \frac{2}{3}\begin{bmatrix} 1 & -\frac{1}{2} & -\frac{1}{2} \\ 0 & \frac{\sqrt{3}}{2} & -\frac{\sqrt{3}}{2} \end{bmatrix}\begin{bmatrix} u_a \\ u_b \\ u_c \end{bmatrix} \tag{2}$$

The space vector is expressed in stationary coordinate, which is denoted by subscript $\alpha\beta$ of the vector itself and composed of α- and β-components [16]. The qd-transformed space vector corresponding to $u_{\alpha\beta}$ is denoted by subscript qd and with components denoted by subscripts q and d, respectively. The relation of transformation between stationary coordinate and synchronous coordinate can be given by

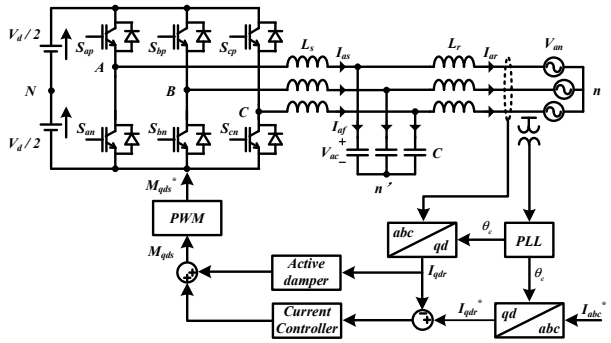

Figure 1: Three-phase LCL-based grid-tied voltage-source-converter with grid-current feedback active damping.

$$u_{qd} = u_q - ju_d = e^{-j\theta_e}u_{\alpha\beta} \Leftrightarrow u_{\alpha\beta} = e^{j\theta_e}u_{qd} \tag{3}$$

$$\begin{bmatrix} u_q \\ u_d \end{bmatrix} = \begin{bmatrix} \cos\theta_e & \sin\theta_e \\ \sin\theta_e & -\cos\theta_e \end{bmatrix} \begin{bmatrix} u_\alpha \\ u_\beta \end{bmatrix} \tag{4}$$

where $\dot{\theta}_e = \omega_e$ is the fundamental angular frequency.

Suppose that we have an input-output relation in stationary as $y_{\alpha\beta} = pu_{\alpha\beta}$, where $p = d/dt$ is the derivative operator which is substituted for Laplace variable *s* whenever a transfer function or matrix is used as an operator. Transformation to the synchronous coordinate $u_{\alpha\beta} = e^{j\theta_e}u_{qd}$ and $y_{\alpha\beta} = e^{j\theta_e}y_{qd}$ yields $y_{qd} = e^{-j\theta_e}p\left(e^{j\theta_e}u_{qd}\right)$. According to the chain rule, $p\left(e^{j\theta_e}u_{qd}\right) = p\left(e^{j\theta_e}\right)u_{qd} + e^{j\theta_e}pu_{qd} = e^{j\theta_e}(p + j\omega_e)u_{qd}$, which gives the relation of transformation by

$$y_{\alpha\beta} = pu_{\alpha\beta} \Leftrightarrow y_{qd} = (p + j\omega_e)u_{qd} \tag{5}$$

Transformation to the synchronous coordinate gives the system model in which the complex transfer function is frequency translated as $s \to s + j\omega_e$.

B. System Model

The diagram for the system considered is depicted in **Figure 1** which illustrates a three-phase LCL-based grid-tied voltage-source-converter with active damping control. A constant DC voltage V_d is assumed for simplicity. Parasitic resistances have been ignored to arrive at the worst case condition. The Phase-Lock-Loop (PLL) has been employed to extract the phase angle of grid V_g, which has also been considered as an ideal AC-source. For the current regulation, a proportional-integral (PI) controller $G_c(s)$ is used as the current controller, represented in the reference-frame by

$$G_c(s) = k_p\left(1 + \frac{1}{\tau_i s}\right) \tag{6}$$

where k_p and τ_i are proportional gain and integral time constant, respectively. $G_2(s)$ is for the active damper, whose transfer function is denoted as

$$G_2(s) = \frac{k_2 s}{s + \omega_2} \tag{7}$$

Where, k_2 and ω_2 are gain and cutoff frequency of HPF.

Assume the DC-bus voltage is divided into two halves by a neutral point of *N*, as shown in **Figure 1**, the state-space description of three-phase LCL-based converter is as in the followings:

$$\begin{cases} V_{AN} = \frac{V_d}{2}\left(2S_{ap} - 1\right) = \frac{V_d}{2}M_{as}^* = L_s pI_{as} + V_{ac} + V_{n'N} \\ V_{BN} = \frac{V_d}{2}\left(2S_{bp} - 1\right) = \frac{V_d}{2}M_{bs}^* = L_s pI_{bs} + V_{bc} + V_{n'N} \\ V_{CN} = \frac{V_d}{2}\left(2S_{cp} - 1\right) = \frac{V_d}{2}M_{cs}^* = L_s pI_{cs} + V_{cc} + V_{n'N} \end{cases} \tag{8}$$

$$\begin{cases} CpV_{ac} = I_{as} - I_{ar} \\ CpV_{bc} = I_{bs} - I_{br} \\ CpV_{cc} = I_{cs} - I_{cr} \end{cases} \tag{9}$$

$$\begin{cases} V_{ac} = L_r pI_{ar} + V_{an} + V_{nn'} \\ V_{bc} = L_r pI_{br} + V_{bn} + V_{nn'} \\ V_{cc} = L_r pI_{cr} + V_{cn} + V_{nn'} \end{cases} \tag{10}$$

Note that $S_{xp}\{x = a, b, c\}$ is the switching function for the top device of *x* phase, and $M_{xs}^*\{x = a, b, c\}$ is the expression of the actual modulation signal of *x* phase.

Taking into account the time delay of the digital control system, the control variables are influenced by the digital time delay [14, 17, 18], which may be modeled as

$$M_{xs}^* = e^{-sT_d}M_{xs}, \qquad x = a, b, c \tag{11}$$

where M_{xs} is the demand control variable. The quantity $T_d = 1.5T_s$ is the total delay time resulting from the digital computation delay (T_s) and the pulse width modulation delay ($0.5T_s$) [14, 18], T_s is the converter sampling period. To obtain a linear state-space model of the pure delay term, an adequate Pade approximation is given by

$$e^{-sT_d} \approx \frac{2 - sT_d}{2 + sT_d} \tag{12}$$

By substituting (12) into (11), the relations between the actual modulation variable and the demand control variable for three-phase quantities can be expressed as

$$\frac{I_{qdr}}{I_{qdr}^* - I_{qdr}} = \frac{k_p\left(1 + \frac{1}{\tau_i s}\right)V_{dc}\left[2 - T_d(s + j\omega_e)\right]}{2\left[2 + T_d(s + j\omega_e)\right](s + j\omega_e)\left[CL_rL_s(s + j\omega_e)^2 + L_r + L_s\right] - \frac{k_2 s}{s + \omega_2}V_{dc}\left[2 - T_d(s + j\omega_e)\right]} \tag{17}$$

$$\frac{I_{qdr}}{I_{qdr}^*} = \frac{k_p\left(s + \frac{1}{\tau_i}\right)(s + \omega_2)V_{dc}\left[2 - T_d(s + j\omega_e)\right]}{k_p\left(s + \frac{1}{\tau_i}\right)(s + \omega_2)V_{dc}\left[2 - T_d(s + j\omega_e)\right] + 2s(s + \omega_2)\left[2 + T_d(s + j\omega_e)\right](s + j\omega_e)\left[CL_rL_s(s + j\omega_e)^2 + L_r + L_s\right] - k_2 s^2 V_{dc}\left[2 - T_d(s + j\omega_e)\right]} \tag{18}$$

This work was supported by National key R & D plan: Research and Demonstration of Key Technology of Charging Facilities Network Combined with Renewable Energy Power Generation (Project No. 2016YFB0900505), and Department of Electrical and Computer Engineering of Tennessee Tech University.

$$\frac{M_{as}^*}{M_{as}} = \frac{M_{bs}^*}{M_{bs}} = \frac{M_{cs}^*}{M_{cs}} = \frac{2 - pT_d}{2 + pT_d} \tag{13}$$

Transforming (8)-(10) and (13) into the synchronous reference frame by using equation (5), a state-space model of three-phase LCL-based converter is given in (14) including the time delay of the digital control system.

$$\begin{cases} \dfrac{V_d}{2} M_{qds}^* = L_s (p + j\omega_e) I_{qds} + V_{qdc} \\ C(p + j\omega_e) V_{qdc} = I_{qds} - I_{qdr} \\ V_{qdc} = L_r (p + j\omega_e) I_{qdr} + V_{qdn} \\ \dfrac{M_{qds}^*}{M_{qds}} = \dfrac{2 - (p + j\omega_e) T_d}{2 + (p + j\omega_e) T_d} \end{cases} \tag{14}$$

The equations can then be converted into the state-space form as

$$p \begin{bmatrix} I_{qds} \\ I_{qdr} \\ V_{qdc} \\ X_{qds} \end{bmatrix} = \begin{bmatrix} -j\omega_e & 0 & -\frac{1}{L_s} & \frac{V_{dc}}{2L_s} \\ 0 & -j\omega_e & \frac{1}{L_r} & 0 \\ \frac{1}{C} & -\frac{1}{C} & -j\omega_e & 0 \\ 0 & 0 & 0 & -\frac{2}{T_d} - j\omega_e \end{bmatrix} \begin{bmatrix} I_{qds} \\ I_{qdr} \\ V_{qdc} \\ X_{qds} \end{bmatrix} + \begin{bmatrix} -\frac{V_{dc}}{2L_s} \\ 0 \\ 0 \\ \frac{4}{T_d} \end{bmatrix} M_{qds} + \begin{bmatrix} 0 \\ -\frac{1}{L_r} \\ 0 \\ 0 \end{bmatrix} V_{qdn} \tag{15}$$

in which the new state is $X_{qds} = M_{qds}^* + M_{qds}$.

For grid-current feedback active damping control as shown in **Figure 1**, the demand control variable is determined by

$$M_{qds} = \left(I_{qdr}^* - I_{qdr}\right) G_c(s) + I_{qdr} G_2(s) \tag{16}$$

And then by solving (15) and (16), the open-loop and closed-loop transfer functions can be expressed by (17) and (18), respectively, which are shown at the bottom of the previous page.

III. CONTROL PARAMETERS DESIGN

The conventional approach toward designing an actively damped system is to design the current controller first, which however can hardly assure the demanded system performance. The method proposed in this paper is to design the current controller and the active damper simultaneously. Four parameters from the two controllers of (6) and (7) must be determined in the design process. And the integral time constant τ_i of (1) is the first parameter to be computed by

$$\tau_i = \frac{10}{\omega_{c(\max)}}, \qquad \omega_{c(\max)} = \frac{\pi - 2\gamma}{6\pi} \omega_s \tag{19}$$

Where, ω_s is the sampling frequency of the system in radian, and $\omega_{c(max)}$ is the maximum crossover frequency [19] in radian corresponding to the defined phase margin of γ which is associated to the relative stability. Note that the PI controller has little phase contribution at the maximum crossover frequency.

With respect to the cutoff frequency ω_2 of (7), noise amplification and digital sampling error realistically limits it to below the Nyquist frequency of $0.5\omega_s$. Observations from [14] are that a high ω_2 is preferable to avoid non-minimum-phase behavior of system, and that a high ω_2 imposes trajectories of closed-loop poles inside and far away from the unit circle altering the dynamic performance of the overall system. The cutoff frequency ω_2 of (7) therefore is set to $0.45\omega_s$ in the paper.

Seen from the closed-loop transfer function of (18), a sixth-order complex system is discussed in the paper, which may not be directly solved for the control parameters. The well-known Routh-Hurwitz criterion is generally the most efficient algorithm to determine whether all the zeros of a characteristic polynomial of the system have negative real parts. However, the extension of the Routh-Hurwitz criterion to polynomials with complex coefficients [20] is much complicated for a high-order system. In order to describe the overall system stability, the D-decomposition [21-23] may therefore be one of the best tools to deal with a complex high-order system, which can be easily employed for providing stability regions graphically. By substituting $s = j\omega$ into the characteristic polynomial of closed-loop transfer function, the boundary of the stability domain is given by the equation

$$a_0(\omega) + a_1(\omega) k_p + a_2(\omega) k_2 + j\left[b_0(\omega) + b_1(\omega) k_p + b_2(\omega) k_2\right] = 0, \quad -\infty < \omega < \infty \tag{20}$$

$$a_0(\omega) = -2\omega(\omega + \omega_e)\left(T_d\omega^2 + T_d\omega_e\omega - 2\omega_2\right)\left[CL_rL_s(\omega + \omega_e)^2 - L_r - L_s\right]$$

$$a_1(\omega) = V_d\omega(T_d\omega\omega_2 + T_d\omega_2\omega e - 2\omega) + \frac{Vd}{\tau_i}\left(T_d\omega^2 + T_d\omega_e\omega + 2\omega_2\right)$$

$$a_2(\omega) = 2V_d\omega^2$$

$$b_0(\omega) = 2\omega(\omega + \omega_e)(T_d\omega\omega_2 + T_d\omega_2\omega_e + 2\omega)\left[CL_rL_s(\omega + \omega_e)^2 - L_r - L_s\right]$$

$$b_1(\omega) = V_d\omega\left(T_d\omega^2 + T_d\omega_e\omega + 2\omega_2\right) - \frac{V_d}{\tau_i}(T_d\omega\omega_2 + T_d\omega_2\omega_e - 2\omega)$$

$$b_2(\omega) = -V_dT_d\omega^2(\omega + \omega_e)$$

in which the imaginary axis (the boundary of instability in the root plane) is mapped into the parameters space. Solving for k_p and k_2

$$\begin{cases} k_p(\omega) = -\dfrac{a_0(\omega)b_2(\omega) - a_2(\omega)b_0(\omega)}{\Delta} \\ k_2(\omega) = \dfrac{a_0(\omega)b_1(\omega) - a_1(\omega)b_0(\omega)}{\Delta} \end{cases} \tag{21}$$

Where, $\Delta = a_1(\omega)b_2(\omega) - a_2(\omega)b_1(\omega)$. By varying ω from negative infinity to positive infinity, a curve of critical stability will be drawn in k_p-k_2 parameter plane.

In designing a control system, it is most important that the system must be stable. Furthermore, it is necessary that the system have adequate relative stability. For indicating the degree of stability of the system, the phase and gain margins are introduced. It should be noted that either the phase margin or the gain margin alone does not give a sufficient indication of the relative stability. Both should be given in the determination

of the relative stability. However, only the phase margin has been discussed in many other works, like in [6,7]. Proper phase and gain margins are to be selected which are robust to parameter changes and ensure closed-loop stability. For satisfactory performance, the phase margin should be between 30° and 60°, and the gain margin should not be less than 6dB [24].

Substituting $s = j\omega$ into the open-loop transfer function of (17), the phase angle φ can be readily determined. HPF gain k_2 of (7) can therefore be computed from:

$$k_2(\omega) = \frac{2(\omega+\omega_e)(\omega^2+\omega_2^2)\left[L_r + L_s - CL_rL_s(\omega+\omega_e)^2\right]}{V_{dc}\omega\left[4+T_d^2(\omega+\omega_e)^2\right]} \times \frac{\left[4-T_d^2(\omega+\omega_e)^2\right]\tan\left(\varphi+\theta(\omega)+\frac{\pi}{2}\right)+4T_d(\omega+\omega_e)}{\omega_2\tan\left(\varphi+\theta(\omega)+\frac{\pi}{2}\right)-\omega} \quad (22)$$

Where, $\theta(\omega)$ is the phase contribution of the PI controller whose notation is given as $\theta(\omega) = \tan^{-1}\left[\omega_{c(max)}/(10\omega)\right]$. Furthermore, the proportional gain of the PI controller k_p of (6) can be determined for selected K_m using equation (23).

$$k_p(\omega) = K_m\sqrt{\frac{n_0(\omega)^2+n_1(\omega)^2}{d_0(\omega)+d_1(\omega)}} \quad (23)$$

$$n_0(\omega) = -2T_d\omega_2(\omega+\omega_e)^2\times\left[L_r+L_s-CL_rL_s(\omega+\omega_e)^2\right] - V_dT_dk_2\omega(\omega+\omega_e)$$

$$n_1(\omega) = -4\omega(\omega+\omega_e)\times\left[L_r+L_s-CL_rL_s(\omega+\omega_e)^2\right] - 2V_dk_2\omega$$

$$d_0(\omega) = V_dT_d\omega(\omega+\omega_e)$$

$$d_1(\omega) = 2V_d(\omega+\omega_2) - V_dT_d\omega_2(\omega+\omega_e)$$

By varying the value of ω in (22) and (23), a curve of correlation between k_p and k_2 can be drawn associated to the defined phase angle and magnitude of the open-loop transfer function. With respective to the definition of the phase margin, we have the following relations:

$$\begin{cases}\gamma = \pi + \varphi \\ K_m = 1\end{cases} \quad (24)$$

And for the gain margin, we have another set of relations as

$$\begin{cases}\varphi = -\pi \\ K_g(dB) = -20\log K_m\end{cases} \quad (25)$$

Note that both sets of different relations will be used for plotting the curves of defined phase margin and defined gain margin of the system, respectively.

IV. Study Cases

For the grid-side current control scheme, many literatures have demonstrated that the active damping is identified as essential for control loop stability in the low resonance frequency region where the resonance frequency of the LCL-filter is lower than 1/6 of the sampling frequency of the system. Active damping is identified as not being required in the higher resonance frequency region in which resonance frequency is high than 1/6 of the sampling frequency. At the critical resonance frequency where these regions cross over (resonance frequency equals to 1/6 of sampling frequency), it is essentially not possible to design a current regulator with an effective damping [7]. This paper addressed this issue by setting three study cases whose resonance frequencies are located in high resonance frequency region, low resonance frequency region, and at the critical resonance frequency, respectively. **Table I** shows the system parameters for the study cases.

TABLE I. LCL-Base System Parameters

Nominal System Parameters		
V_d	DC bus voltage	380V
V_g	Grid phase RMS voltage	120V
f_e	System fundamental frequency	60Hz
f_{sw}	Switching frequency	5kHz
f_s	Sampling frequency	10kHz
***LCL*-filter Parameters**		
L_s = 8.4mH		L_r = 2.5mH
Case A	C = 2.1uF	f_{res} = 2.50kHz > f_s / 6
Case B	C = 4.6uF	f_{res} = 1.69kHz ≈ f_s / 6
Case C	C = 16uF	f_{res} = 0.91kHz < f_s / 6

TABLE II. Controller Parameters

Test Case	PI (k_p)	PI (τ_i)	HPF (k_2)	HPF (ω_2)
Case A				
K_g = 6dB	0.1969	$120/\omega_s$	0.1626	$0.45\omega_s$
K_g = 3dB	0.2409		0	
Case B				
K_g = 6dB	0.1153	$120/\omega_s$	0.4651	$0.45\omega_s$
K_g = 3dB	0.1515		0.2894	
Case C				
K_g = 3dB	0.0552	$120/\omega_s$	0.6611	$0.45\omega_s$

For sufficient performance, the phase margin γ is set to be 45°, and the gain margin K_g is set to be 6dB. Applying the D-composition tool, the critical boundary can be determined at first, which divides the parameter plane into two parts of stable region inside and unstable region outside. And then a curve associated with the specified phase margin can be drawn to identify the trace where phase margin is 45°. The last step is to identify the trace for the gain margin of 6dB. **Figure 2** shows all possibilities for control parameters due to these specifications. It should be noted that as the resonance frequency increases, the region of stability reduces.

In **Figure 2(a)**, the GM line of 6dB coincides with the PM line at two points. However, the point denoted by *o* is invalid since it is beyond the stable region. Note that the active damping contributes a more degree of stability for Case A, though active damping is not essential. In **Figure 2(b)**, two intersections are within the stable region. The point denoted by x is chosen since it has a bigger PI gain which can provide a

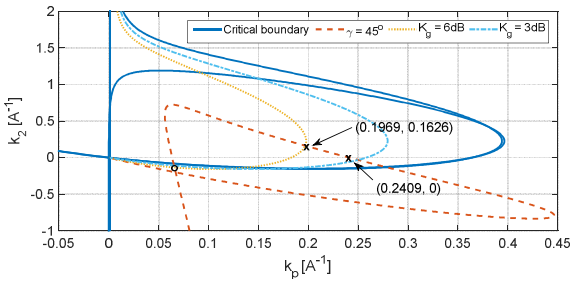

(a) Case A

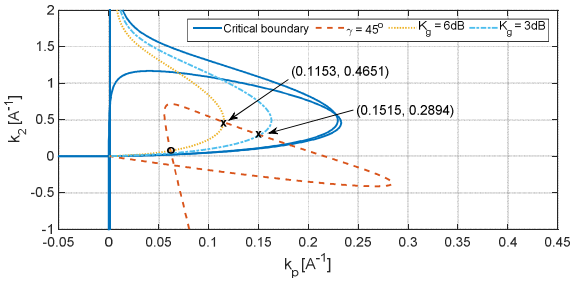

(b) Case B

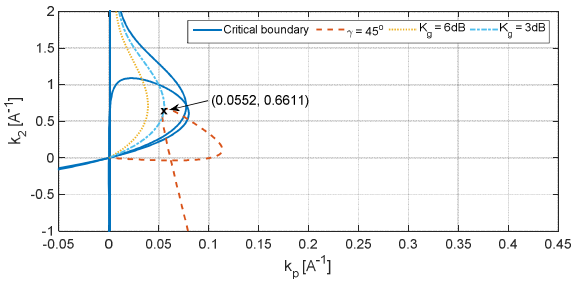

(c) Case C

Figure 2: Loci of the controller parameters between k_p and k_2 for the three study cases.

wider system bandwidth, leading to a faster system response. In **Figure 2(c)**, there is no intersection between the GM line of 6dB and the PM line. It implies that it is not always possible to design a current regulator for Case C to meet both relative stability requirements, no matter whether an active damping scheme is introduced. To address this issue, a compromised gain margin of 3dB is applied. A compromised gain margin contributes to a smaller HPF gain k_2 and a larger PI gain k_p, so as to readily meet the gain margin requirement for Case A with no use of active damping. However, a small gain margin may weaken the robustness of the system. All controller parameters determined graphically from **Figure 2** are summarized in **Table II**. With the summarized parameters, bode plots of open-loop transfer functions are drawn for the adequate gain margin of 6dB and the compromised gain margin of 3dB, respectively. From **Figure 3**, the 45° phase margin can be readily identified. However, only Case A and B can meet the 6dB gain margin requirement, shown in **Figure 3(a)**. The Bode plot frequency respond for Case A without an active damping is shown in Figure 3(b) to meet the 3dB gain margin, as well Case B and C with an active damping.

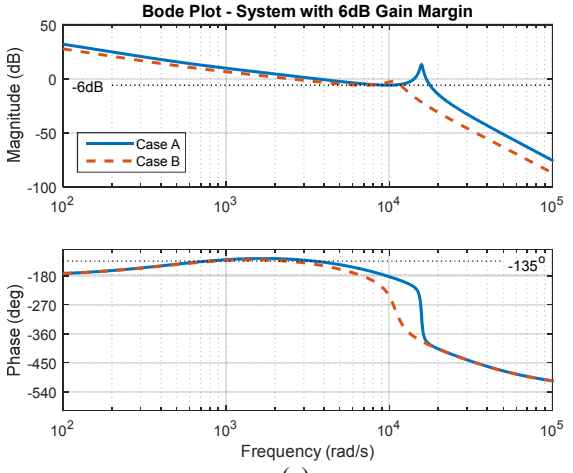

(a)

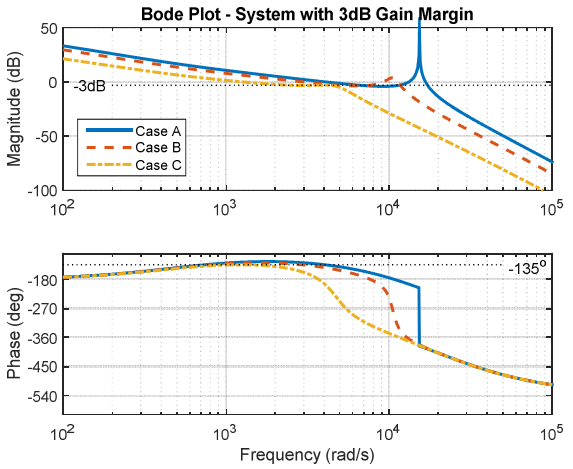

(b)

Figure 3: Bode plots of the open loop transfer function for case A, B and C: (a) 6dB gain margin; (b) 3dB gain margin.

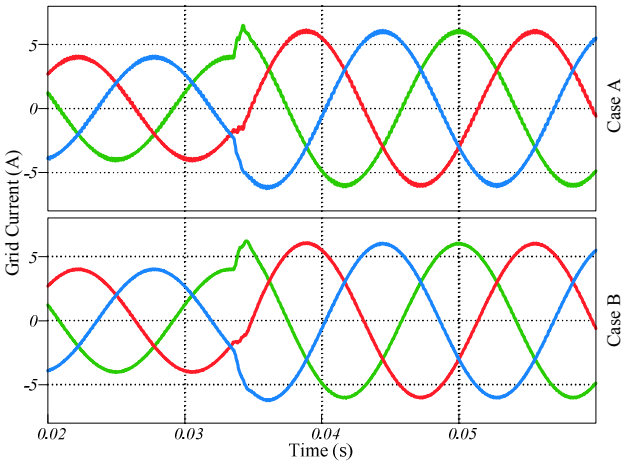

Figure 4: Simulation results of grid-current responses for the systems with 45° phase margin and 6dB gain margin.

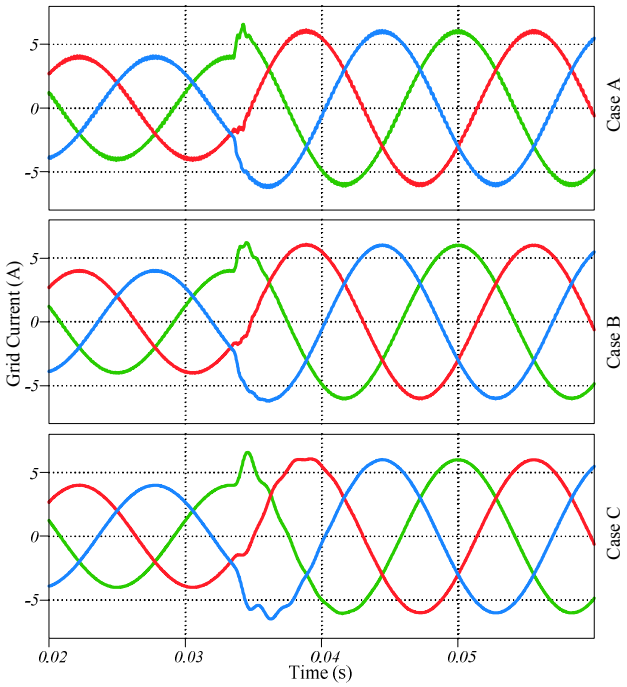

Figure 5: Simulation results of grid-current responses for the systems with 45° phase margin and 3dB gain margin.

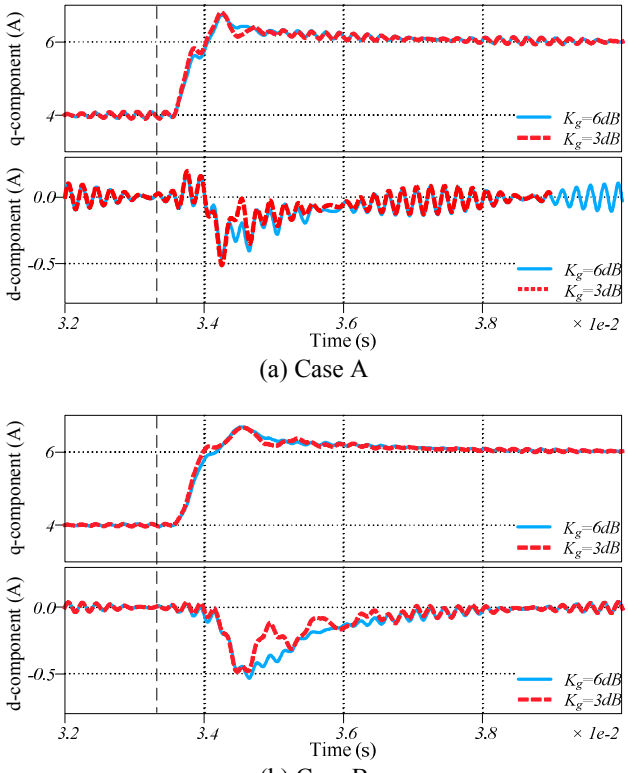

(a) Case A

(b) Case B

Figure 6: Simulation result comparisons of the q- and d-component of the grid-currents under different gain margin conditions.

V. Simulation Results

The implementation of the proposed design method for the three study cases (A, B and C) of **Table I** is simulated with piecewise linear electrical circuit simulation (PLECS). Controller parameters considered are taken from **Table II**. Transient time-domain system responses are shown in **Figure 4** and **Figure 5**. For each case, a step change in commanded peak current from 4 to 6 A is used to demonstrate the system dynamic performance. **Figure 4** shows that the system responds with sufficient gain margin for Case A and B, where the grid-currents are well damped during the time of transition, and little oscillations are produced. Corresponding to the case with the compromised gain margin, the system responses for three study cases are shown in **Figure 5**. Compared with the responses of the systems with sufficient gain margins, more oscillations are found during the transient event. It is noted that when the resonance frequency is low, the settling time is longer

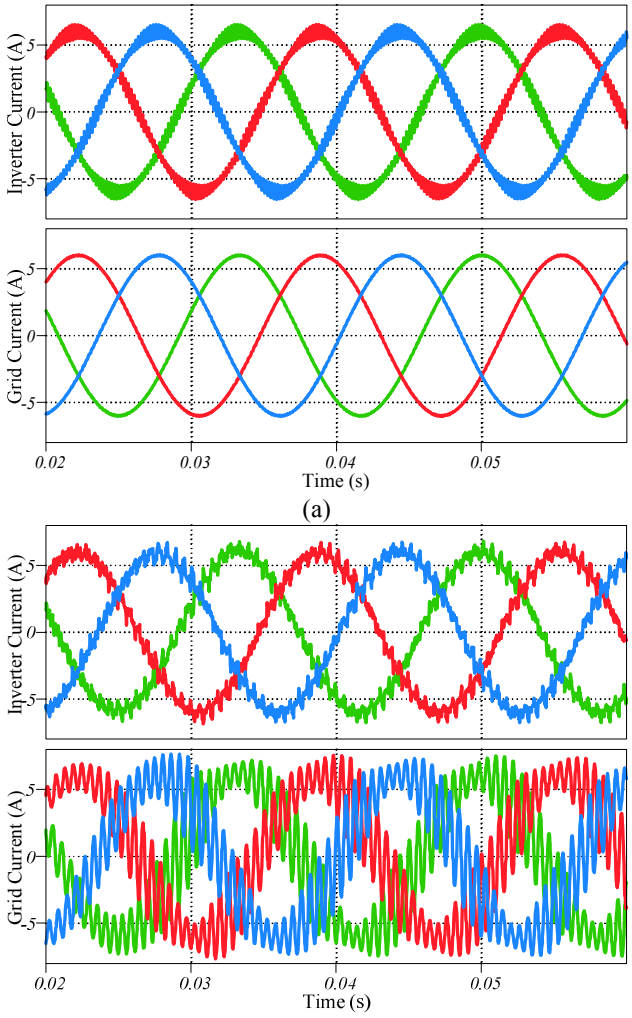

(a)

(b)

Figure 7: Simulation of system in Case A when grid-side inductance is double. (a) Control parameters associated to 6dB gain margin; (b) Control parameters associated to 3dB gain margin.

under the same relative stability conditions. Especially, for Case C shown in **Figure 5**, more than a half fundamental period is required to settle the grid-currents. In order to easily compare the responses of the currents between different gain margins, the q- and d-components of the grid-currents are given in **Figure 6** for Case A and B, respectively. It demonstrates that the larger PI gains can lead to a faster grid current response.

The grid-side inductance is now doubled and the gain margins retained as the nominal values in case A. It turns out that the system whose control design is done with the higher gain margin has more stability margin and provides stronger system robustness, as demonstrated in **Figure 7**.

VI. Experimental Results

For further verification, the three-phase LCL-based grid-tied inverter shown in **Figure 1** was implemented in the Laboratory. Circuit parameters used for the setup are listed in **Table I**, while **Table II** lists the parameters of the PI controllers and active damper designed using the proposed concurrent design method. The designed control scheme was eventually implemented using a DSP of TMS320F28335 as the controller for sampling the grid-current feedback signals and generating the modulation pulses.

With the implemented setup, **Figure 8** shows the measured grid currents for Case A listed in Table **I** using different controlling parameters. Since the resonance frequency of the LCL filter is higher than the critical resonance frequency (f_s / 6), the system remains stable even when no active damping is activated, as demonstrated in **Figure 8(a)** with k_2 = 0. However, the system dynamics can be improved by specifying a higher gain margin, as shown in **Figure 8(b)**. Corresponding experimental results for Case B and C are given in **Figures 9** and **10**, respectively. **Figure 9** shows that the system with a higher gain margin has a better system dynamics when the active damping is essentially required. **Figure 10** shows the controlled grid side currents when the resonance frequency is lower than the critical resonance.

VII. Conclusions

In this paper, a novel concurrent design scheme based on the D-decomposition methodology was proposed for the current control design with active damping of LCL-based grid-tied VSC converter using the grid-current feedback only. Unlike other conventional methods, an accurate defined phase margin and gain margin can be met easily. Proposed design also demonstrates that the grid-current active damping technique can provide satisfactory system performance independent of the resonance frequency. The overall controller design is quite intuitive and graphical, and no expertise parameter tuning is need, which thus is ideal for non-expert use or for adaption of different configurations. Simulation and experimental results have demonstrated the validity and effectiveness of the proposal.

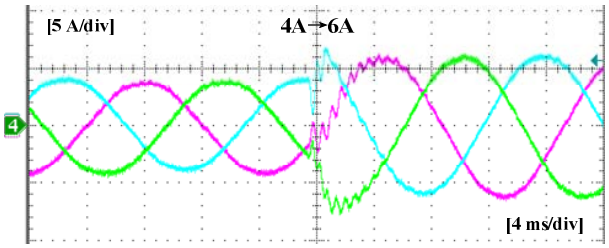

(a)

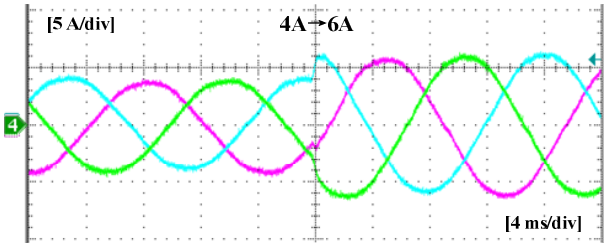

(b)

Figure 8: Experimental results of grid-current responses for Case A with: (a) 3dB gain margin; (b) 6dB gain margin.

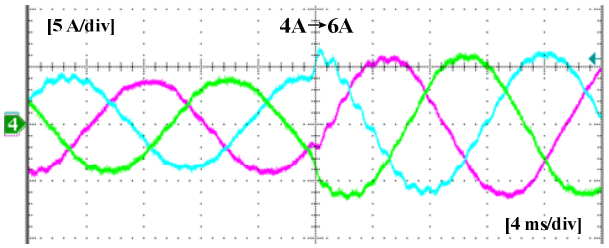

(a)

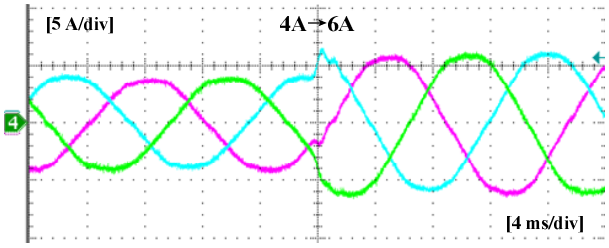

(b)

Figure 9: Experimental results of grid-current responses for Case B with: (a) 3dB gain margin; (b) 6dB gain margin.

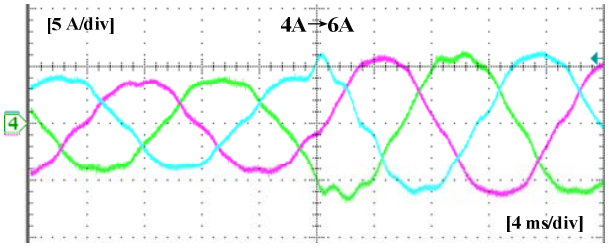

Figure 10: Experimental results of grid-current responses for Case B with 3dB gain margin.

REFERENCES

[1] M. Liserre, F. Blaabjerg and S. Hansen, "Design and control of an LCL-filter-based three-phase active rectifier," *IEEE Transactions on Industry Applications*, vol. 41, no. 5, pp. 1281-1291, Sept.-Oct. 2005.

[2] J. Yin, S. Duan and B. Liu, "Stability analysis of grid-connected inverter with LCL filter adopting a digital single-loop controller with inherent damping characteristic," *IEEE Transactions on Industrial Informatics*, vol. 9, no. 2, pp. 1104-1112, May 2013.

[3] C. Zou, B. Liu, S. Duan and R. Li, "Influence of delay on system stability and delay optimization of grid-connected inverters with LCL filter," *IEEE Transactions on Industrial Informatics*, vol. 10, no. 3, pp. 1775-1784, Aug. 2014.

[4] J. Wang, J. D. Yan, L. Jiang and J. Zou, "Delay-dependent stability of single-loop controlled grid-connected inverters with LCL filters," *IEEE Transactions on Power Electronics*, vol. 31, no. 1, pp. 743-757, Jan. 2016.

[5] J. Yin, S. Duan and B. Liu, "Stability analysis of grid-connected inverter with LCL filter adopting a digital single-loop controller with inherent damping characteristic," *IEEE Transactions on Industrial Informatics*, vol. 9, no. 2, pp. 1104-1112, May 2013.

[6] Z. Xin, X. Wang, P. C. Loh and F. Blaabjerg, "Grid-current-feedback control for LCL-filtered grid converters with enhanced stability," *IEEE Transactions on Power Electronics*, vol. 32, no. 4, pp. 3216-3228, April 2017.

[7] S. G. Parker, B. P. McGrath and D. G. Holmes, "Regions of active damping control for LCL filters," *IEEE Transactions on Industry Applications*, vol. 50, no. 1, pp. 424-432, Jan.-Feb. 2014.

[8] F. Liu, Y. Zhou, S. Duan, J. Yin, B. Liu and F. Liu, "Parameter design of a two-current-loop controller used in a grid-connected inverter system with LCL filter," *IEEE Transactions on Industrial Electronics*, vol. 56, no. 11, pp. 4483-4491, Nov. 2009.

[9] Y. Tang, P. C. Loh, P. Wang, F. H. Choo, F. Gao and F. Blaabjerg, "Generalized design of high performance shunt active power filter with output LCL filter," *IEEE Transactions on Industrial Electronics*, vol. 59, no. 3, pp. 1443-1452, March 2012.

[10] J. Dannehl, F. W. Fuchs, S. Hansen and P. B. Thogersen, "Investigation of active damping approaches for PI-based current control of grid-connected pulse width modulation converters with LCL filters," *IEEE Transactions on Industry Applications*, vol. 46, no. 4, pp. 1509-1517, July-Aug. 2010.

[11] B. Bahrani, M. Vasiladiotis and A. Rufer, "High-order vector control of grid-connected voltage-source converters with LCL-filters," *IEEE Transactions on Industrial Electronics*, vol. 61, no. 6, pp. 2767-2775, June 2014.

[12] M. Hanif, V. Khadkikar, W. Xiao and J. L. Kirtley, "Two degrees of freedom active damping technique for LCL filter-based grid connected PV systems," *IEEE Transactions on Industrial Electronics*, vol. 61, no. 6, pp. 2795-2803, June 2014.

[13] J. Xu, S. Xie and T. Tang, "Active damping-based control for grid-connected LCL-filtered inverter with injected grid current feedback only," *IEEE Transactions on Industrial Electronics*, vol. 61, no. 9, pp. 4746-4758, Sept. 2014.

[14] X. Wang, F. Blaabjerg and P. C. Loh, "Grid-current-feedback active damping for LCL resonance in grid-connected voltage-source converters," *IEEE Transactions on Power Electronics*, vol. 31, no. 1, pp. 213-223, Jan. 2016.

[15] R. Fantino, C. Busada and J. Solsona, "Optimum PR control applied to LCL filters with low resonance frequency," *IEEE Transactions on Power Electronics* , vol.33, no.99, pp.1-1

[16] L. Harnefors, "Modeling of three-phase dynamic systems using complex transfer functions and transfer matrices," *IEEE Transactions on Industrial Electronics*, vol. 54, no. 4, pp. 2239-2248, Aug. 2007.

[17] X. Chen, X. Ruan, D. Yang, W. Zhao and L. Jia, "Injected grid current quality improvement for a voltage-controlled grid-connected inverter," *IEEE Transactions on Power Electronics*, vol. 33, no. 2, pp. 1247-1258, Feb. 2018.

[18] Y. Wang, X. Wang, F. Blaabjerg and Z. Chen, "Harmonic instability assessment using state-space modeling and participation analysis in inverter-fed power systems," *IEEE Transactions on Industrial Electronics*, vol. 64, no. 1, pp. 806-816, Jan. 2017.

[19] D. G. Holmes, T. A. Lipo, B. P. McGrath and W. Y. Kong, "Optimized design of stationary frame three phase ac current regulators," *IEEE Transactions on Power Electronics*, vol. 24, no. 11, pp. 2417-2426, Nov. 2009.

[20] A. Dòria-Cerezo, M. Bodson, C. Batlle and R. Ortega, "Study of the stability of a direct stator current controller for a doubly fed induction machine using the complex hurwitz test," *IEEE Transactions on Control Systems Technology*, vol. 21, no. 6, pp. 2323-2331, Nov. 2013.

[21] D. D. Siljak, Nonlinear systems-the parameter analysis and design, John Wiley & Sons, New York, 1969

[22] E. N. Gryazina and B. T. Polyak, "Stability regions in the parameter space: D-decomposition revisited," *Automatica*, vol. 42, no. 1, pp.13-26, Jan. 2006.

[23] E. N. Gryazina, B. T. Polyak and A. A. Tremba, "D-decomposition technique state-of-the-art," *Automation and Remote Control*, vol. 69, no. 12, pp. 1991-2026, Dec. 2008.

[24] K. Ogata, Modern control engineering (5th edition), Pearson, Cambridge, 2009